On-chip three-dimensional tumor spheroid formation and pump-less perfusion culture using gravity-driven cell aggregation and balanced droplet dispensing

Taeyoon Kim,[a] Il Doh, and Young-Ho Cho[b]
Cell Bench Research Center, KAIST, Daejeon, South Korea

(Received 10 May 2012; accepted 12 July 2012; published online 24 July 2012)

This paper presents a spheroid chip in which three-dimensional (3D) tumor spheroids are not only formed by gravity-driven cell aggregation but also cultured at the perfusion rates controlled by balanced droplet dispensing without fluidic pumps. The previous spheroid chips require additional off-chip processes of spheroid formation and extraction as well as bulky components of fluidic pumps. However, the present spheroid chip, where autonomous medium droplet dispensers are integrated on a well array, achieves the on-chip 3D tumor spheroid formation and perfusion culture using simple structure without bulky fluidic pumps. In the experimental study, we demonstrated that the spheroid chip successfully forms 3D tumor spheroids in the wide diameter range of 220 μm–3.2 mm (uniformity $> 90\%$) using H358, H23, and A549 non-small cell lung cancer cells. At the pump-less perfusion culture ($Q = 0.1$–0.3 μl/min) of spheroids, the number of H358 cells in the spheroid increased up to 50% from the static culture ($Q = 0$ μl/min) and the viability of the cultured cells also increased about 10%. Therefore, we experimentally verified that the perfusion environment created by the spheroid chip offers a favourable condition to the spheroids with high increase rate and viability. The present chip achieves on-chip 3D tumor spheroid formation and pump-less perfusion culture with simple structure, thereby exhibiting potential for use in integrated *in-vivo*-like cell culture systems.
© *2012 American Institute of Physics*. [http://dx.doi.org/10.1063/1.4739460]

I. INTRODUCTION

Bio-assays with three-dimensional (3D) multi-cellular spheroids are crucial for recent cell-based biomedical research and clinical studies since 3D spheroid culture provides more accurate *in-vivo*-like microenvironments[1] compared to two-dimensional (2D) monolayer culture. 3D tumor spheroids, resembling *in-vivo* tumor nodules, are used for recent cancer research to recapitulate cancer cell proliferation and necrosis,[2] multi-cellular chemo-resistance,[3] cell metastasis,[4] drug penetration,[5] etc. Recent cancer research[6] also verifies that the gene expression of 3D tumor spheroids is more similar to clinical expression profiles than that of 2D monolayer. Thus, a simple and effective method of 3D tumor spheroid formation and culture is essential for current cancer research.

Conventionally, the hanging-drop method[7,8] has been widely used for the formation of 3D tumor spheroids in biomedical cancer research. However, the 3D tumor spheroids formed by the hanging-drop method should be extracted and seeded into other culture devices to implement the perfusion culture of spheroids. Therefore, the conventional hang-drop method requires additional off-chip processes of spheroid formation and extraction. Recently, a number of microfluidic spheroid chips have been developed to implement the on-chip formation and culture of 3D tumor spheroids. However, the previous spheroid chips[9–13] still utilize static cell culture, thus rendering

[a]Current affiliation: Process Methodology Development Group, Samsung Electromechanics Co., Ltd.
[b]Author to whom correspondence should be addressed. Electronic mail: nanosys@kaist.ac.kr.

 © 2012 American Institute of Physics

them incapable of creating *in-vivo*-like microenvironments where bio-molecules such as nutrients and waste products are continuously flowing through the cells. Other spheroid chips[14–21] were developed to perform the perfusion cell culture, but the bulky fluidic pumps were still required for precise control of perfusion rate, thus making it difficult to create a compact integrated chip. In this paper, we present a spheroid chip in which autonomous medium droplet dispensers are integrated on a well array, performing the on-chip 3D tumor spheroid formation and pump-less perfusion culture with simple structure.

II. THEORETICAL STUDY

A. Working principle

The spheroid chip, illustrated in Fig. 1, consists of two poly-dimethylsiloxane (PDMS) layers: a well layer and a droplet dispenser layer. The overall dimensions of the well layer and the droplet dispenser layer are 85 mm × 56 mm and 75 mm × 56 mm, respectively. The well layer (Fig. 1(a)) has a 4 × 8 array of 6 mm-diameter wells, where eight wells in each row are interconnected to a common drain port through drain channels. We have designed the diameter and pitch of the wells as 6 mm and 9 mm, respectively, compatible to those of the conventional

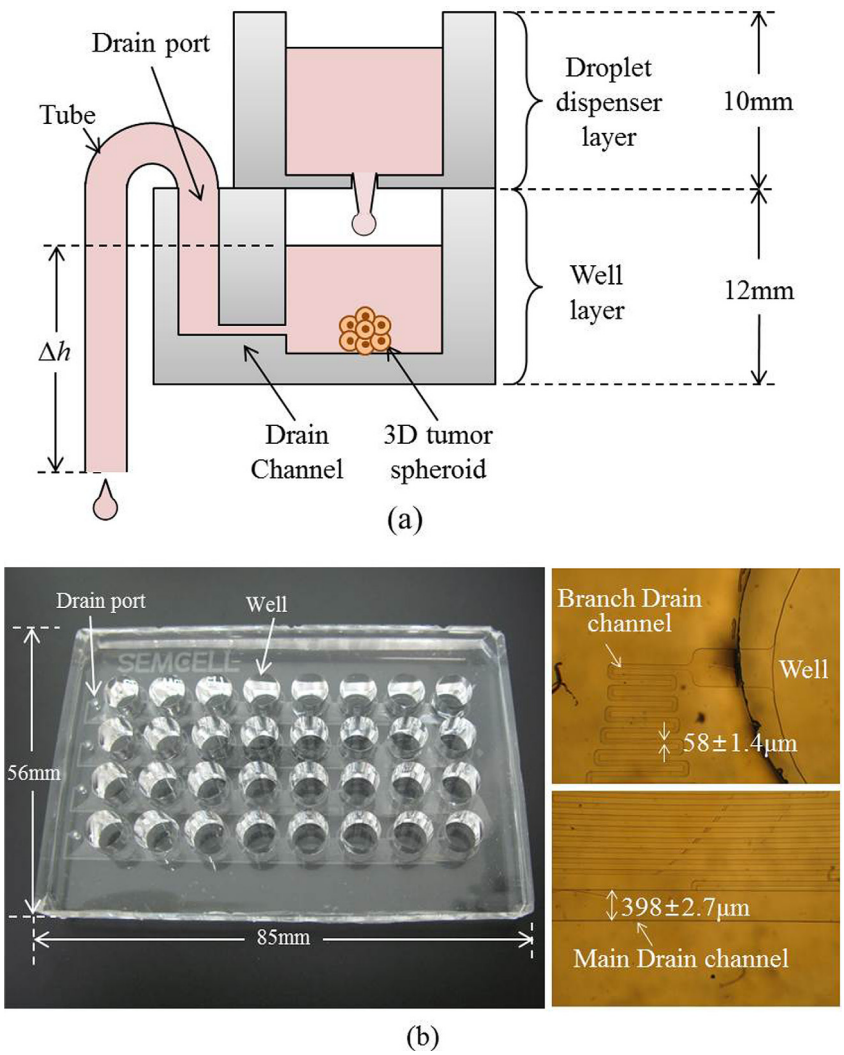

FIG. 1. On-chip 3D tumor spheroid formation and pump-less perfusion culture spheroid chip: (a) cross-sectional view of a unit well; (b) overall view of fabricated prototypes with enlargement of drain channel.

96-well plate. The droplet dispenser layer (Fig. 1(b)), where dispenser tips are plugged at the bottom, is placed on top of the well layer to supply fresh medium droplets to the wells through the dispenser tips.

Figure 2(a) shows the 3D tumor spheroid formation using the spheroid chip of Fig. 1. We seed cells in the well array and place the chip upside down so that the cells aggregate each other due to the gravitational force in the suspended medium droplet. After incubating the cells to form 3D tumor spheroids, we place the chip upright and remove surplus medium. Assuming the 3D tumor spheroid has a perfectly spherical shape, we derive the spheroid diameter, D, as

$$D = \sqrt[3]{n/\alpha} \cdot d, \tag{1}$$

where n, d, and α are the number, the diameter, and the packing density of cells in a spheroid, respectively. The packing density, α, is defined as 0.36 (Ref. 22) for common cancer cells.

After the 3D tumor spheroid formation, the spheroid chip cultures the cells at the constant medium perfusion rate (Fig. 2(b)) using the previously developed autonomous droplet dispensing method.[23] The gravity-driven perfusion flow, Q, generated by the hydraulic-head difference, Δh, between the well-inlet and the drain-outlet, results in the removal of waste droplets at the drain. Since the removed waste droplet expands the air trapped in the wells, the air pressure drops below the ambient pressure. Therefore, the droplet dispenser autonomously replenishes the well with a medium droplet in the amount of the removed waste droplet, then the air pressure returns to an ambient pressure. Consequently, the spheroid chip maintains the constant hydraulic-head difference, Δh, thus performing the constant flow rate medium perfusion without requiring fluidic pumps.

B. Drain channel design

The eight wells in each row of the 4×8 well array (Fig. 1(a)) are interconnected to a common drain port by main and branch drain channels. The fluidic resistance, R_b, of the branch

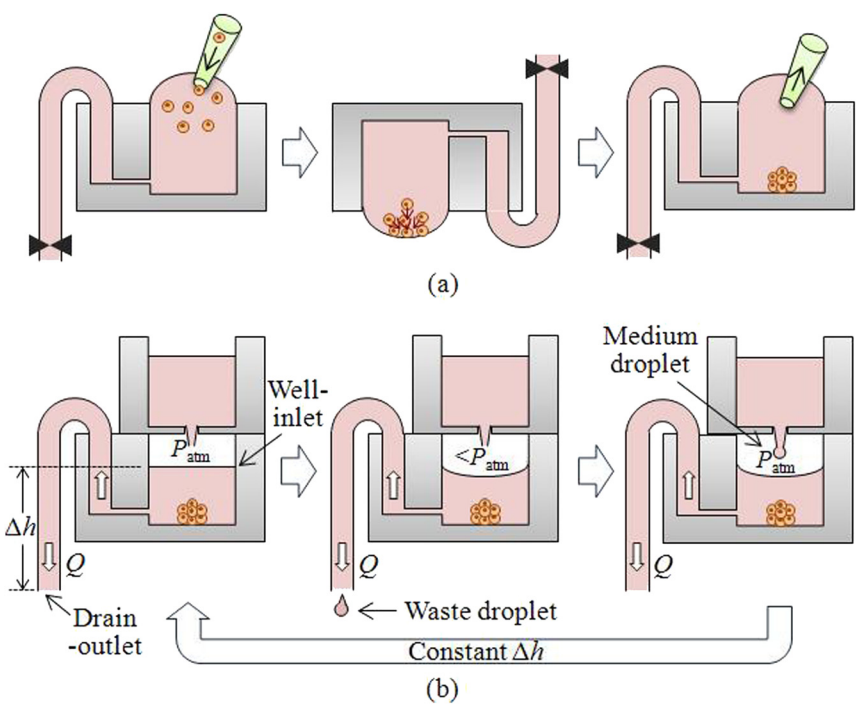

FIG. 2. Working principle of the spheroid chip: (a) spheroid formation using the gravity-driven cell aggregation; (b) pump-less perfusion culture of the spheroids using balanced droplet dispensing.

drain channel should be sufficiently higher than that, R_m, of the main drain channel in order to obtain uniform perfusion rates, $Q_1 \sim Q_8$, for the eight different wells in Fig. 1(a). Here, the branch drain channel is designed to have 600 times higher fluidic resistance than that of the main channel (R_b:$R_m = 600$:1). Since we have designed the fluidic resistance of the main drain channel, R_m, to be negligible compared to that of the branch drain channel, R_b, the perfusion rate for the wells can be simplified as

$$Q \approx \frac{\rho g \Delta h}{R_b}, \tag{2}$$

where ρ and g are the medium density and the gravitational acceleration, respectively. Therefore, the perfusion rate, Q, can be controlled by adjusting the hydraulic-head difference, Δh. At the hydraulic-head difference, Δh, in the range of 33 mm–100 mm, the perfusion rate, Q, is designed to be generated as 0.1 μl/min–0.3 μl/min, which is a widely used range for the perfusion cell culture.[24] As a result, the fluidic resistance, R_m and R_b, of the main and branch drain channels is determined as 3.09×10^{11} Pa·s m^{-3} and 1.87×10^{14} Pa·s m^{-3}, respectively. In order to obtain the fluidic resistance of R_m and R_b, we have designed the dimensions of the main and branch drain channels as 400 μm (width) $\times$ 220 μm (height) $\times$ 72 mm (length) and 60 μm (width) $\times$ 60 μm (height) $\times$ 85 mm (length), respectively.

III. FABRICATION

The fabrication process of the spheroid chip is composed of three processing steps: (1) droplet dispenser layer fabrication, (2) well layer fabrication, and (3) device assembly. We fabricated the droplet dispenser layer from the moulding and bonding processes of two PDMS plates. The 8 mm-thick top plate of the droplet dispenser layer was fabricated by moulding PDMS pre-polymer in an acrylic jig with a 4×8 array of 6 mm-diameter pillars. The PDMS pre-polymer mixture (curing agent-to-PDMS ratio of 1:10, Sylgard 184, Dow Corning), degassed in a vacuum chamber, was poured into the acryl jig. After curing the PDMS for 12 h at 75 °C, we peeled the PDMS top plate from the acrylic jig. The 3 mm-thick bottom plate of the droplet dispenser layer was obtained by curing 24 g of PDMS pre-polymer mixture on a 4-in. bare silicon wafer for 2 h at 85 °C. We bonded the top and bottom PDMS plates of the droplet dispenser layer by treating the bonding surfaces with O_2 plasma for 30 s. Then, we plugged a 2 mm-long polypropylene tip at the center of each well bottom after perforating a 1 mm-diameter hole by using a puncher.

The well layer was fabricated from the similar PDMS moulding and bonding processes for the droplet dispenser layer. The 8 mm-thick top plate of the well layer was fabricated by curing PDMS pre-polymer in the identical acrylic jig for the droplet dispenser layer. We fabricated the drain channel mould by the two-step lithography process of 60 μm and 160 μm-thick SU-8 photoresists (Microchem, Newton, MA) on a 4 in. silicon wafer. Then, the 4 mm-thick bottom plate of the well layer was fabricated by curing 30 g PDMS pre-polymer for 2 h at 85 °C on the SU-8 drain channel mould. We bonded the fabricated top and bottom plates after treating the bonding surfaces with O_2 plasma for 30 s.

We sterilized the fabricated droplet dispenser layer and well layer by an autoclave and dried them overnight. Then, the bottom surfaces of the wells were treated with 2 wt. % bovine serum albumin (BSA) solution for 1 h at room temperature to prevent the cell adhesion. After formation of spheroid in the well layer (Fig. 2(a)), we stacked the droplet dispenser layers on top of the well layer and sealed them using an acrylic jig with a bolted joint for perfusion culture as shown in Fig. 2(b). In order to ensure the identical hydraulic head difference, Δh, in all wells, we adjusted the volume of media to 140 μl in all wells and fixed the height of drain tubes by using a jig (Fig. 1(b)).

We measured the dimension of the drain channels and obtained the fluidic resistance, R_m and R_b, of the main and branch drain channels as 3.13×10^{11} Pa·s m^{-3} and 2.24×10^{14} Pa·s m^{-3}, respectively. Based on the fluidic resistance of the fabricated drain channels, we determined the

hydraulic-head difference, Δh, as 0, 38, 76, and 114 mm for generating the perfusion rate, Q, of 0, 0.1, 0.2, and 0.3 μl/min, respectively.

IV. EXPERIMENTAL METHODS AND PROTOCOLS

A. Cell preparation

In the experimental study, we used H358, H23, and A549 non-small cell lung cancer (NSCLC) cell lines, which were obtained from ATCC (American Type Culture Collection). Among the three cell lines, the H358 cells were stably transfected by green fluorescence protein (GFP) to facilitate the cell image analysis. The H23 and A549 cells were cultured in complete media consisting of RPMI-1640 (Gibco) supplemented with 10% (v/v) fetal bovine serum (FBS; Gibco) and 1% (v/v) penicillin-streptomycin (Invitrogen). For the H358 cells, we additionally supplemented the culture media with 0.2% (v/v) G418 solution (Sigma Aldrich) to maintain the cells stably transfected with GFP. The cells were cultured in a humidified 37 °C and 5% CO_2 incubator and routinely passaged at 80% confluence. We collected the cells by treating the culture dish with 0.25% trypsin/EDTA (Invitrogen) for 3 min at 37 °C and then neutralized the cell solution with 10% RPMI-1640 medium (Gibco). After spinning down the cells with a centrifuge at 1500 rpm for 3 min, we resuspended the cells in fresh medium. We adjusted the number of cells by measuring the cell concentration with a hemocytometer (Marienfeld) and seeded the cells in the chip by using a micropipette (Eppendorf).

B. Cell increase and viability measurement

After culturing the 3D tumor spheroids in the chip, we disaggregated the cultured spheroids into single cells by treating the spheroids with 0.25% trypsin/EDTA for 15 min at 37 °C. Then, we characterized the increase rate by measuring the number of cells with a hemacytometer (Marienfeld). The increase rate was calculated based on the equation

$$\text{cell increase rate}\,(\%/\text{d}) = \frac{n_f - n_i}{n_i} \times 100/\Delta t, \tag{3}$$

where n_i is the initial number of cells in a spheroid measured at day 0 of the perfusion culture and n_f is the final number of cells in a spheroid measured after the total culture duration, Δt, of 18 days. The cell viability was characterized by staining the disaggregated cells with Ethidium homodimer (EthD-1, Invitrogen) after the 18 days of perfusion culture. The cells were treated with 4 μM EthD-1 in an incubator for 45 min at 37 °C. As a result, dead cells were stained with EthD-1 and appeared to be red while normal GFP-stable H358 cells only expressed green fluorescence. The cell viability was calculated as

$$\text{cell viability}(\%) = \frac{\textit{Number of live cells}}{\textit{Number of total cells}} \times 100, \tag{4}$$

where the number of live and total cells were measured using MATLAB® image processing tools.

C. Histological analysis of 3D tumor spheroids (H&E staining)

The status of cells in the spheroid center was characterized by staining the 3D tumor spheroid slices with hematoxylin and eosin (H&E). 3D spheroids were fixed with 4% formalin for 10 min and washed with deionised water for 1 h. Then, we successively dipped and washed the spheroids with 70%, 80%, 90%, 95%, and 100% (3 times) ethanol, each for 5 min, and finally treated the spheroids with a 100% ethanol and xylene mixture (volume ratio = 1:1) and xylene (2 times), each for 5 min. The spheroids were extracted and embedded in a paraffin block and sectioned to 3 μm-thick slices. We stained the spheroid slices with hematoxylin and eosin and then analyzed the cell packing status by observing the stained spheroid slices with an inverted microscope (Axiovert 25, Carl Zeiss).

V. EXPERIMENTAL RESULTS AND DISCUSSION

In the experimental study, we characterized the 3D tumor spheroid formation and perfusion culture performance using H358, H23, and A549 NSCLC cells. In the spheroid formation test, we measured the size range and uniformity of 3D tumor spheroids formed of eight different numbers of H358, H23, and A549 cells. In the spheroid culture test, we measured the increase and viability of H358 cells in three different sizes of 3D tumor spheroids cultured at four different perfusion rates for 18 days. We also investigated the cause of the spheroid size-dependent cell growth rate and viability variation by observing the cell status in the spheroid center.

A. 3D tumor spheroid formation

We measured the size range and uniformity of the 3D tumor spheroids formed of H358, H23, and A549 human lung cancer cells at the various initial numbers of cancer cells: 5×10^2, 10^3; 5×10^3, 10^4; 5×10^4, 10^5; and 5×10^5, 10^6. The cancer cells were loaded in the wells, and different sizes of spheroids were formed depending on the initial cancer cell numbers. Figure 3(a) shows the microscopic images of the 3D tumor spheroids formed of H358, H23, and A549 cells using the gravity-driven aggregation for 5 days in the CO_2 incubator. Analyzing the projected area of the 3D tumor spheroids using the MATLAB® image processing tool, we measured the spheroid diameter (Fig. 3(b)) as a function of the number of cells. In the graph of Fig. 3(b), the average and standard deviation of the spheroid diameters were obtained from four different spheroids for each number of cells. As a result, the 3D tumor spheroid diameter was measured in the range of 220 μm–3.2 mm with a uniformity higher than 90%. Therefore, we experimentally verified that the spheroid chip successfully forms the spheroids in the wide size range of 220 μm–3.2 mm, which is comparable to the 200 μm–1 mm required for spheroid-based drug-screening.[25] We also observed that the measured diameter of 3D tumor spheroids formed of H358 cells agrees well with the theoretical estimation of Eq. (1) (the solid line in Fig. 3(b)) within the error of less than 4.94%. However, the H23 and A549 cells showed relatively large discrepancies of 28.3% and 54.6%, respectively, between the measured and theoretical spheroid diameters. The cell line-dependent spheroid size error is due to the difference in the cell-to-cell interaction properties: H358 cells have tight cell-to-cell interaction with the abundant cell adhesion molecules, such as E-cadherin,[24] thus forming 3D tumor spheroids in a spherical shape similar to the theoretical model of Eq. (1). However, the cell-to-cell interaction of H23 and A549 cells is relatively weak due to the lack of E-cadherin molecules at the cell membranes.[26] Therefore, the loose cell-to-cell interaction of H23 and A549 cells resulted in the formation of oblate 3D tumor spheroids rather than the perfectly spherical spheroids as in Eq. (1).

B. 3D tumor spheroid culture

We formed 209.6 ± 9.46, 376.4 ± 15.8, and 535.7 ± 21.2 μm-diameter 3D tumor spheroids using the 5 days of gravity-driven aggregation for 10^3, 5×10^3, and 10^4 H358 cells, respectively. Then, we cultured the 3D spheroids in a 37 °C and 5% CO_2 humidified incubator at the

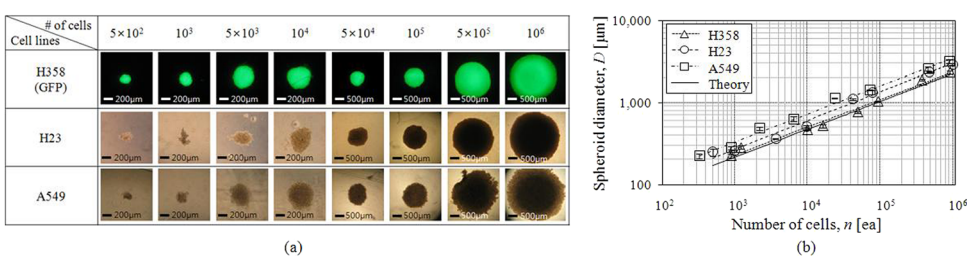

FIG. 3. 3D tumour spheroids formed by the different numbers of H358, H23, and A549 human lung cancer cells: (a) microscopic images of the spheroids; (b) experimental and theoretical spheroid diameters as a function of the number of cells; the solid line in the graph of (b) indicates the theory of Eq. (1).

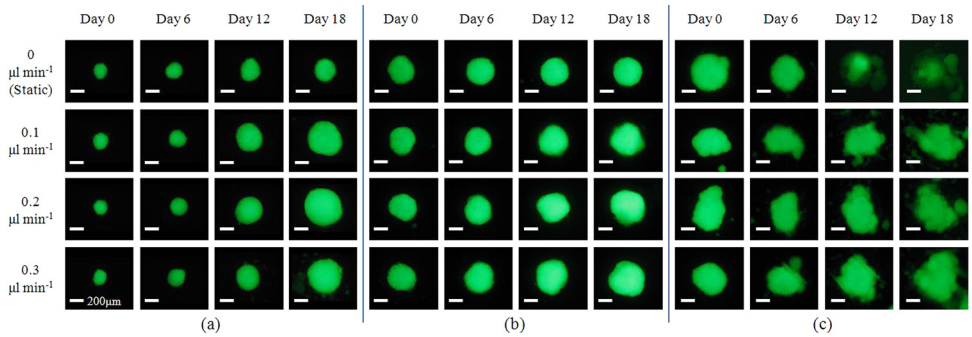

FIG. 4. Time-lapse fluorescence images of the 3D tumour spheroids, formed by H358 cell numbers of (a) 10^3, (b) 5×10^3, and (c) 10^4, cultured for 18 days at the four different perfusion rates of 0, 0.1, 0.2, and 0.3 μl/min.

perfusion rates, Q, of 0, 0.1, 0.2, and 0.3 μl/min which are generated from the balanced droplet dispensing in Fig. 2(b). Figure 4 shows the time-lapse fluorescent H358 spheroid images captured by an inverted fluorescent microscope (Axiovert 25, Carl Zeiss) at the intervals of 6 days for a total duration of 18 days. By measuring the diameter of H358 spheroids using the MATLAB® image processing tool, we obtained the spheroid growth pattern, as shown in Fig. 5. In the graph of Fig. 5, the average and standard deviation of the H358 spheroid diameters were measured from three different spheroids at each perfusion rate. We observed that the 3D tumor spheroids formed of H358 cells steadily grew at the perfusion culture ($Q = 0.1$ μl/min–0.3 μl/min), but the spheroids in the static culture ($Q = 0$ μl/min) showed a relatively slow growth pattern. Especially, the diameter of large spheroids, initially formed of 10^4 H358 cells, could not be measured after the 12 days of static culture since the spheroids were disaggregated into several parts.

After the total 18 days of culture, we disaggregated the H358 spheroids into single cells by treating the spheroids with 0.25% trypsin/EDTA for 10 min at 37 °C. Figure 6 shows the correlation between the number of H358 cells, n, and the 3D tumor spheroid diameter, D, measured at the start point (day 0) and the end point (day 18) of perfusion culture at four different perfusion rates, Q, of 0, 0.1, 0.2, and 0.3 μl/min. In the graph of Fig. 6, the average and standard deviation of the H358 cells and the 3D tumor spheroid diameters were obtained from three different spheroids at each perfusion rate. The dashed lines in the graphs of Fig. 6 indicate the theoretical relation between the number of cells and the 3D tumor spheroid diameter based on Eq. (1). As a result, we observed that the correlation between the number of H358 cells and the 3D tumor spheroid diameter agrees with the theory of Eq. (1). The spheroid growth in Fig. 6(b) indicated that the size of spheroid is mostly originated by the increase of packing density of cancer cells. Further biological researches are required to be performed for understanding the spheroid growth depending on the number of cells.

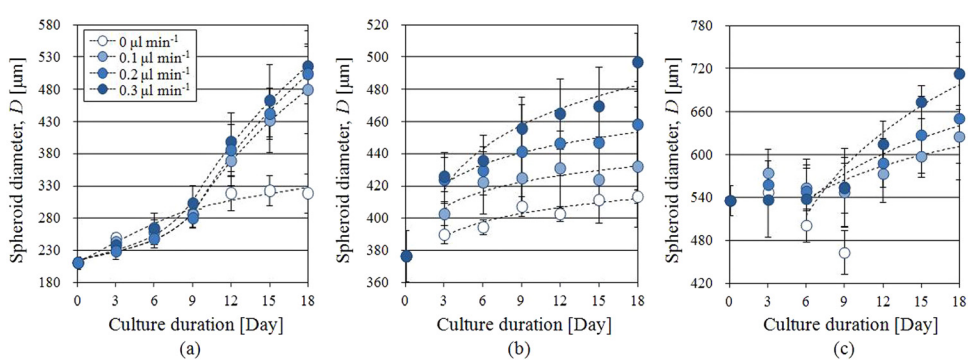

FIG. 5. Diameter of 3D tumour spheroids, formed by H358 cell numbers of (a) 10^3, (b) 5×10^3, and (c) 10^4, cultured for 18 days at the four different perfusion rates of 0, 0.1, 0.2, and 0.3 μl/min.

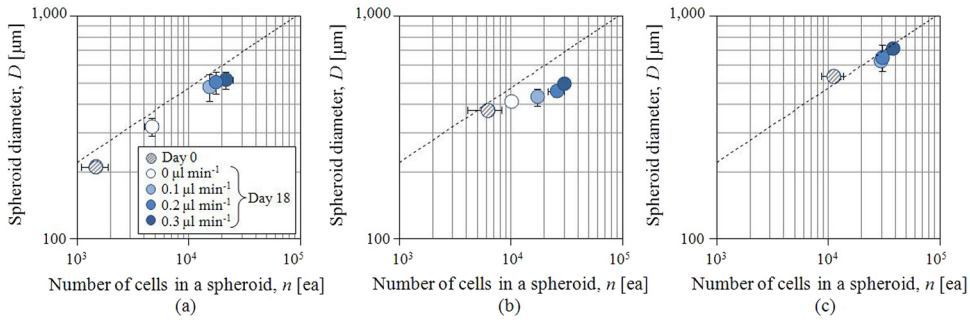

FIG. 6. Correlation between the number of H358 cells and the spheroid diameter measured at day 0 and day 18 of culture at the four different perfusion rates of 0, 0.1, 0.2, and 0.3 μl/min; the dashed lines in the graphs indicate the theoretical relation based on Eq. (1).

Based on the numbers of H358 cells measured at day 0 and day 18 of the perfusion culture, we obtained the increase rate of Eq. (3), as shown in Fig. 7(a). In the graph of Fig. 7(a), the average and standard deviation of the increase rate were obtained from four measurements at each perfusion rate. At the perfusion culture ($Q = 0.1\ \mu$l/min–$0.3\ \mu$l/min), the H358 spheroids with the initial diameters of 209.6 ± 9.46, 376.4 ± 15.8, and $535.7 \pm 21.2\ \mu$m showed average increase rates of 62.5, 16.4, and 10.7% d^{-1}, respectively, which were higher than 12.0, 3.61, and 0.24% d^{-1} of static culture ($Q = 0\ \mu$l/min). This suggests that the perfusion culture provided more favourable culture environments to the spheroids than the static culture[24] by facilitating the efficient nutrients supply as well as waste product removal.

From the graph of Fig. 7(a), we also observed that the number of H358 cells decreased as the 3D tumor spheroid size increased. In order to investigate the cause of spheroid size-

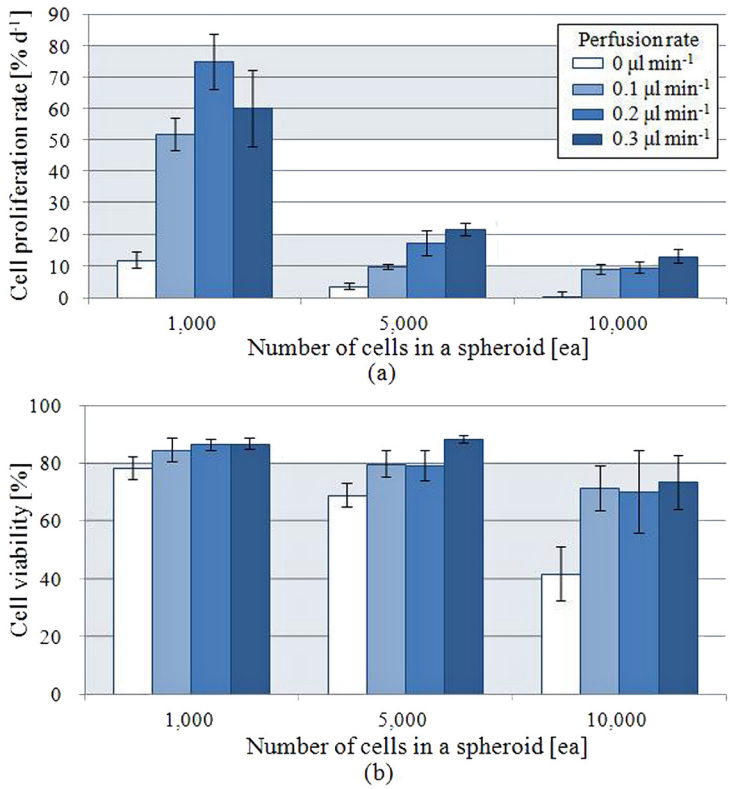

FIG. 7. Increase rate and viability measured after the 18 days culture of H358 spheroids depending on the perfusion rate and the number of cells: (a) increase rate; (b) viability.

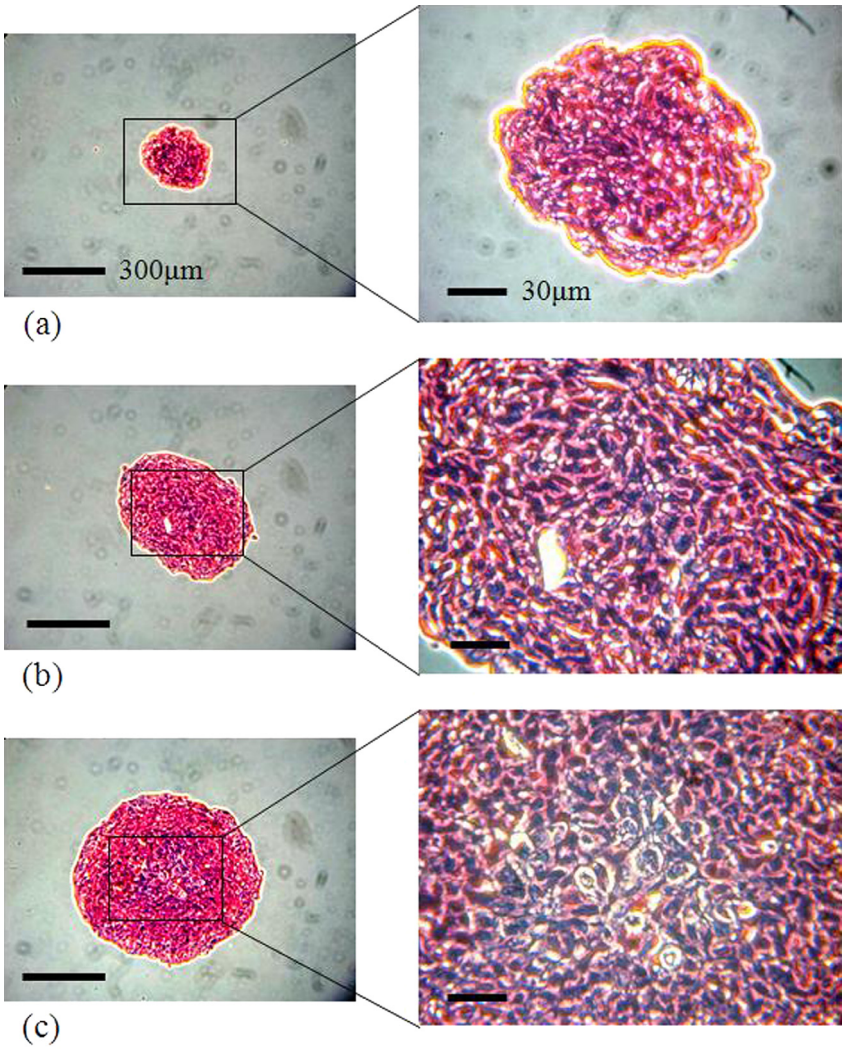

FIG. 8. Microscopic images of the 3D tumour spheroids, formed by H358 cell numbers of (a) 10^3, (b) 5×10^3, and (c) 10^4, stained with hematoxylin and eosin after the 18 days of static culture.

dependent increase rate variation, we characterized the status of H358 cells in the spheroid center through the histological analysis of hematoxylin and eosin (H&E) staining (Fig. 8). The 3D tumor spheroids, formed by H358 cells at the numbers of 10^3, 5×10^3, and 10^4 for 5 days and static cultured for 18 days, were used in the H&E staining test. The H358 cells in the small 3D tumor spheroids ($D = 242.0\,\mu$m and $456.3\,\mu$m) showed the densely packed morphologies (Figs. 8(a) and 8(b)), but the H358 cells at the center of the large spheroid ($D = 634.3\,\mu$m) showed loose density (Fig. 8(c)). In order to examine the specific effect of spheroids size on the proliferation characteristics, further BrdU staining test is required to be performed.

C. Cell viability

To evaluate the viability of H358 cells in the 3D tumor spheroids cultured for 18 days, we disaggregated the spheroids and stained the single cells with $4\,\mu$M EthD-1 for 45 min at 37 °C. By analyzing the stained cell images, we measured the viability of Eq. (4) for the H358 cells in the three different size 3D tumor spheroids depending on the perfusion rates, Q, of 0, 0.1, 0.2, and $0.3\,\mu$l/min (Fig. 7(b)). In the graph of Fig. 7(b), the average and standard deviation of the cell viability were obtained from three measurements at each perfusion rate. At the perfusion culture ($Q = 0.1\,\mu$l/min–$0.3\,\mu$l/min), the H358 spheroids with the initial diameters of

209.6 ± 9.46, 376.4 ± 15.8, and $535.7 \pm 21.2\,\mu$m showed the average cell viability of 85.9%, 82.4%, and 71.6%, respectively. Compared to the static culture ($Q = 0\,\mu$l/min), the viabilities were increased by 7.5%–29.9% depending on the size of the spheroid. Therefore, we experimentally demonstrated that the perfusion environment created by the spheroid chip offers a favourable condition to the spheroids with high viability. We also observed that the H358 cell viability decreased as the 3D spheroid size increased.

VI. CONCLUSIONS

We have designed, fabricated, and characterized the spheroid chip, where the on-chip 3D tumor spheroid formation and pump-less perfusion culture are achieved by gravity-driven cell aggregation and balanced droplet dispensing. In the experimental study, we demonstrated that the spheroid chip successfully forms 3D tumor spheroids in the wide diameter range of $220\,\mu$m–3.2 mm (uniformity $> 90\%$) using H358, H23, and A549 human lung cancer cells. At the pump-less perfusion culture ($Q = 0.1$–$0.3\,\mu$l/min) of spheroids, the number of H358 cells increased up to 50% from the static culture ($Q = 0\,\mu$l/min) and the viability of the cultured cells also increased about 10%. Therefore, we experimentally verified that the perfusion environment created by the spheroid chip offers a favourable condition to the spheroids with viability. Compared to the previous chips requiring additional off-chip spheroid formation and extraction processes as well as bulky fluidic components, the present chip achieves the on-chip 3D tumor spheroid formation and pump-less perfusion culture with simple structure. Therefore, the present spheroid chip has potential for use in the integrated *in-vivo*-like cell culture systems.

ACKNOWLEDGMENTS

This research was supported by the Converging Research Center Program funded by the Ministry of Education, Science, and Technology (Project No. 2011K000864).

[1]F. Pampaloni, E. G. Reynaud, and E. H. K. Stelzer, Nat. Rev. Mol. Cell Biol. **8**, 839–845 (2007).
[2]R. C. Bates, N. S. Edwards, and J. D. Yates, Crit. Rev. Oncol. Hematol. **36**, 61–74 (2000).
[3]F. Hirschhaeuser, H. Menne, C. Dittfeld, J. West, W. Mueller-Klieser, and L. A. Kunz-Schughart, J. Biotechnol. **148**, 3–15 (2010).
[4]M. A. dit Faute, L. Laurent, D. Ploton, M.-F. Poupon, J.-C. Jardillier, and H. Bobichon, Clin. Exp. Metastasis **19**, 161–168 (2002).
[5]A. I. Minchinton and I. F. Tannock, Nat. Rev. Cancer **6**, 583–592 (2006).
[6]P. C. De Witt Hamer, A. A. G. Van Tilborg, P. P. Eijk, P. Sminia, D. Troost, C. J. F. Van Noorden, B. Ylstra, and S. Leenstra, Oncogene **27**, 2091–2096 (2008).
[7]J. M. Kelm, N. E. Timmins, C. J. Brown, M. Fussenegger, and L. K. Nielsen, Biotechnol. Bioeng. **83**, 173–180 (2003).
[8]T. Tamura, Y. Sakai, and K. Nakazawa, J. Mater. Sci.: Mater. Med. **19**, 2071–2077 (2008).
[9]D. Wlodkowic, S. Faley, J. Skommer, D. McGuinness, and J. M. Cooper, Anal. Chem. **81**, 9828–9833 (2009).
[10]Y. Markovitz-Bishitz, Y. Tauber, E. Afrimzon, N. Zurgil, M. Sobolev, Y. Shafran, A. Deutsch, S. Howitz, and M. Deutsch, Biomaterials **31**, 8436–8444 (2010).
[11]Y.-S. Torisawa, A. Takagi, Y. Nashimoto, T. Yasukawa, H. Shiku, and T. Matsue, Biomaterials **28**, 559–566 (2007).
[12]Y.-C. Tung, A. Y. Hsiao, S. G. Allen, Y.-S. Torisawa, M. Ho, and S. Takayama, Analyst **136**, 473–478 (2011).
[13]J. Lee, M. J. Cuddihy, G. M. Cater, and N. A. Kotov, Biomaterials **30**, 4687–4694 (2009).
[14]Y.-S. Torisawa, B.-H. Chueh, D. Huh, P. Ramamurthy, T. M. Roth, K. F. Barald, and S. Takayama, Lab Chip **7**, 770–776 (2007).
[15]A. Y. Hsiao, Y.-S. Torisawa, Y.-C. Tung, S. Sud, R. S. Taichman, K. J. Pienta, and S. Takayama, Biomaterials **30**, 3020–3027 (2009).
[16]L. Yu, M. C. W. Chen, and K. C. Cheung, Lab Chip **10**, 2424–2432 (2010).
[17]L. Y. Wu, D. Di Carlo, and L. P. Lee, Biomed. Microdevices **10**, 197–202 (2008).
[18]Y.-S. Torisawa, B. Mosadegh, G. D. Luker, M. Morell, K. S. O'Shea, and S. Takayama, Integr. Biol. **1**, 649–654 (2009).
[19]C. Kim, K. S. Lee, J. H. Bang, Y. E. Kim, M.-C. Kim, K. W. Oh, S. H. Lee, and J. Y. Kang, Lab Chip **11**, 874–882 (2011).
[20]K. Lee, C. Kim, J. Young Yang, H. Lee, B. Ahn, L. Xu, J. Yoon Kang, and K. W. Oh, Biomicrofluidics **6**, 14114–141147 (2012).
[21]J. Fukuda and K. Nakazawa, Biomicrofluidics **5**, 22205 (2011).
[22]D. Khaitan, S. Chandna, M. B. Arya, and B. S. Dwarakanath, J. Transl. Med. **4**, 12 (2006).
[23]T. Kim and Y.-H. Cho, Lab Chip **11**, 1825–1830 (2011).
[24]L. Kim, Y.-C. Toh, J. Voldman, and H. Yu, Lab Chip **7**, 681–694 (2007).
[25]J. Friedrich, C. Seidel, R. Ebner, and L. A. Kunz-Schughart, Nat. Protoc. **4**, 309–324 (2009).
[26]S. Thomson, E. Buck, F. Petti, G. Griffin, E. Brown, N. Ramnarine, K. K. Iwata, N. Gibson, and J. D. Haley, Cancer Res. **65**, 9455–9462 (2005).